Influence of natural organic matter fractions on PAH sorption by stream sediments and a synthetic graphene wool adsorbent

Adedapo O. Adeola [a] and Patricia B.C. Forbes [a*]

[a]*Department of Chemistry, Faculty of Natural and Agricultural Sciences, University of Pretoria, Lynnwood Road, Hatfield, Pretoria 0002, South Africa*.

Abstract

The sorption of selected PAHs onto sediment components and graphene wool were studied. Different natural organic matter (NOM)- mineral-deficient (MDF), mineral-rich (MRF), and black carbon (BCF) fractions were recovered from natural sediment (NAS) using sequential separation methods. Detailed characterization of sediment components using BET, ICP-OES, SEM-EDS, XRD, and FTIR were carried out and significant changes in the physicochemical properties of sorbents due to the treatment procedure were revealed. Experimental data showed that a pseudo-second-order and Freundlich adsorption model best fit kinetic and isotherm studies, validated by the least values of Error Sum of Squares (SSE). Isotherm data revealed that complementary processes involving both multilayer adsorption and partitioning of PAHs occurred. NAS, BCF, and MDF with higher % OC had higher Freundlich and maximum adsorption capacities (K_f and q_{max}) than MRF for PAHs and an *S*-type sorption curve ($N > 1$) dominated the PAH-NOM interaction, with few exceptions for LMW PAHs. MRF significantly diminished the efficiency of graphene wool in the removal of selected PAHs from aqueous solution, as both adsorption capacity (K_d) and efficiency reduced from 16.9 g L^{-1} and 95.4 % to 0.3 g L^{-1} and 18.5 % respectively. Sorption of the selected PAHs was slightly favored under acidic pH and higher temperatures. The sorption reaction was endothermic for NAPH & PHEN, and exothermic for PYR & PERY. Furthermore, aromaticity and hydrophobic moieties of the different PAHs and NOM significantly influenced the π-π and hydrophobic-organophilic interactions that may have occurred, which led to some degree of irreversible sorption as shown by *H*-indices. Therefore, the probable impact of each NOM fraction on the mobility and environmental risk management/remediation of PAHs is herewith evaluated.

Keywords: *graphene wool; isotherm; kinetics; natural organic matter (NOM); polycyclic aromatic hydrocarbons (PAHs); sorption process*

1.0. Introduction

Polycyclic aromatic hydrocarbons (PAHs) are a ubiquitous and potentially carcinogenic class of environmental contaminants (ECs), composed of compounds with several aromatic rings (Gupta and Kumar, 2020). In South Africa, the total concentrations of PAHs in Buffalo River were in the range of 14.91-206 µg L^{-1} (in water) and 1107-22,310 µg kg^{-1} (in sediment) (Adeniji et al., 2019), while as high as 8,310 µg L^{-1} was detected in wastewater influents (Limpopo province) (Mojiri et al., 2019). Natural organic matter (NOM) is a heterogeneous mixture of organic compounds, which are present in water supplies and a trace amount in treated water (Mahato and Gupta, 2020). NOM is either an amorphous or condensed phase of carbon, also referred to as hard carbon, soot, black carbon, coal-derived particles, etc., which have been reported in natural sediments either as dissolved organic carbon (DOC) and/or particulate organic carbon (POC) and they have been postulated to be responsible for the desorption resistance and recalcitrance of contaminants in water bodies (Karickhoff et al., 1979; Kraaij et al., 2003; Ran et al., 2007).

In the environment, strong interactions exist between several hydrophobic organic contaminants (HOCs) and natural organic matter (NOM), and this plays a vital role in their fate, mobility, human exposure risk, and toxicity in aquatic environments. Furthermore, the bioavailability, pollution potential, and persistence of sediment-bound hydrophobic organic compounds depend on their physicochemical properties and partitioning between the solid and aqueous interphase is indicative of potential risk with respect to recontamination of water bodies (Ghosh et al., 2001; Lu and Pignatello, 2002). Thus, there is a need to study the sorption-desorption interactions between different fractions of NOM and PAHs.

The efficiency of treatment strategies for PAH polluted aquatic environment is influenced by the PAHs bound to sediment, which could potentially partition into the aqueous phase. Thus, to

establish the fate and possible remediation strategy suitable for different classes of environmental contaminants in water, including PAHs, the amount of PAH adsorbed onto sediment components/NOMs must be accounted for (Ran et a., 2007; Ololade et al., 2018). In the last decade, graphene has attracted scientific interest in technological development for the remediation of polluted water, either in its pristine condition or as composites (Singh et al., 2018; Adeola and Forbes, 2019; Das et al., 2020). Therefore, since NOM in untreated water leads to the fouling of pipelines and membrane filters used in water treatment plants (Yu et al., 2018; Mahato and Gupta, 2020); it is imperative to study the influence of different fractions of NOM on the adsorption performance of graphene wool.

This study aims at providing insights into the mechanisms of adsorption of PAHs onto sediment components, and the release potential of adsorbed PAHs into waters bodies and aquifers. Delineation of condensed and amorphous phases of NOM as well as understanding the role of *in-situ* mineral enrichment on the overall adsorption of two-to-five ringed PAHs, are all vital aspects of this study. This investigation will also provide useful information on how the presence of different NOM will potentially influence the efficiency of synthetic graphene-based materials (GBMs) used for water treatment purposes.

2.0. Materials and Methods

2.1. Chemicals

Neat standards (98% purity) of naphthalene (NAPH), phenanthrene (PHEN), pyrene (PYR), and perylene (PERY) were purchased from Supelco (USA). PAHs are hydrophobic compounds; however, their solubility can be ensured using established procedures (Crisafully et al., 2008). The

stock solutions were prepared by dissolving a known weight of PAH neat standard in 30% (v/v) methanol in deionized water to promote the dissolution of the respective PAHs.

Sodium azide (NaN_3) was purchased from Sigma-Aldrich (Germany), nitric acid (HNO_3), hydrochloric acid (HCl), sodium chloride (NaCl), sodium hydroxide (NaOH), and calcium chloride ($CaCl_2$) were purchased from Associated Chemical Enterprises (ACE, Johannesburg, South Africa). Sterile syringe filters (33 mm diameter) with a 0.45µm pore size containing a hydrophilic polyethersulfone (PES) membrane were purchased from Merck (Darmstadt, Germany). All the solutions were prepared with ultra-pure water (9.2 µS/cm^3) obtained from a Milli-Q water purification system (Millipore, Bedford, MA, USA).

2.2. Equipment and characterization

Fluorescence emission measurements were taken using a Horiba Jobin Yvon Fluoromax-4 spectrofluorometer (Horiba Instruments Inc., Edison, NJ, USA). Elemental analysis was carried out using inductively coupled plasma-optical emission spectrometry (ICP-OES, Spectro Arcos model, Thermo Fisher Scientific, South Africa). Powder X-ray diffraction (XRD) patterns were obtained using a Bruker, D2 Phaser, Cu (Kα) radiation (λ = 1.54184 Å) (Bruker AXS GmbH, Karlsruhe, Germany). Scanning electron microscopy (SEM) images were taken using a Zeiss Ultra-Plus 55 field emission scanning electron microscope (FE-SEM), operated at 2.0 kV and equipped with an energy dispersive X-ray spectrometer (EDS) (OXFORD Link-ISIS-300 Zeiss, Germany). FTIR spectra were obtained using a Bruker Alpha-T spectrometer (Bruker Optik GmbH, Ettlingen, Germany). The surface area and porous structure of sediment components were determined by N_2 adsorption-desorption isotherms at 77 K, using a NOVA Touch Surface Analyzer system (Anton Paar, South Africa) in a relative pressure (P/P_0) range of 0.01−1.0, following a model of Brunauer−Emmett−Teller (BET) and Barrett−Joyner−Halenda (BJH) techniques. 10 mg of the

NOM fractions were weighed into pre-cleaned crucibles and placed in a muffle furnace (Carbolite™, ThermoFisher Scientific, South Africa) at 350˚C for 16 h. After cooling the samples were re-weighed and the weight difference was used to estimate the organic carbon content (%) (Frangipane et al., 2009; Nelson and Sommers, 2018). Point zero net charge (PZNC) was determined using the salt addition method (Mahmood et al., 2011). A shaking water bath was purchased from Celsius Scientific (South Africa). The ionic strength of solutions was monitored using an Orion Star A112 conductivity benchtop meter (Thermo Scientific, South Africa), and pH was measured using a 780-pH meter (Metrohm Herisau, Switzerland).

2.3. Sediment collection and treatment

Stream sediment was collected from the University of Pretoria sports campus, South Africa (latitude E28° 14′ 46″ and longitude S25° 45′ 10″), using a stainless-steel trowel cleaned with methanol, and samples were transported in clean polypropylene zip-lock bags. Each sediment sample was air-dried for 48 hours at ambient temperature, ground with a clean agate mortar and pestle, and sieved with a mesh size of 54 µm in the laboratory. The sieved sediment was stored in air-tight glass bottles at ambient temperature before further treatment.

The natural sediment (NAS) in addition to three sorbent fractions; mineral-deficient fraction (MDF), black carbon fraction (BCF), and a mineral-rich fraction (MRF) obtained from the NAS sample, were used in this study to evaluate the influence of NOM fractions on sorption of 2- to 5-membered ring PAHs. Briefly, the bulk sediment sample was split into two portions and from one portion, the first isolate (MDF sample) was recovered via the treatment of NAS with 1 N HCl for 45 min at ambient temperature (Ololade et al., 2018). After rinsing with deionized water, the sample was treated with a mixture of 1 N HCl and 10 % HNO_3, three times successively for 12 hr at ambient temperature. The solid residue recovered after centrifuging at 3800 g for 30 min and filtration using

Whatman filter paper (11 µm pore size), was washed with deionized water and freeze-dried at −4 °C for 24 hr (Gelinas et al., 2001). The BCF sample was obtained by thermal oxidation of the MDF sample in a crucible, heated in a tube furnace at 375 °C for 24 hr, where the residue obtained is condensed organic matter, composed of cross-linked heterocyclic compounds (Ran et al., 2007; Ololade et al., 2018). *In-situ* enrichment of minerals in the native sediment (NAS) was done by repeatedly adding 30 % H_2O_2 with stirring at 40 ˚C. This was repeated until the solution became clear, indicating that most of the organic matter had been removed (Mikutta et al., 2005), and the residue (MRF) was rinsed with deionized water and freeze-dried before sorption studies.

2.4. Isotherm sorption experiment

Batch sorption experiments were carried out in sealed 40 mL PTFE screw cap amber vials (Stargate Scientific, South Africa) at 25 ± 1 °C. Background solution (pH = 7.0) contained 0.01 mol L^{-1} $CaCl_2$ (ACE, South Africa) in deionized water with 200 mg L^{-1} NaN_3 (Sigma-Aldrich, Germany) as a biocide. The experiments were conducted in triplicate with varying initial NAPH, PHEN, PYR, or PERY concentrations. Sorption kinetic studies were carried out using 100 mL beakers, sealed with aluminum foil. 20 mg of each adsorbent was treated with 50 mL of NAPH, PHEN, PYR, or PERY (500 µg L^{-1}) in a background electrolyte solution (pH=7 ± 0.1). The vials were equilibrated for 24 hr and supernatants were taken for fluorescence spectrometric analysis at different time intervals. For the isotherm study, each of the bulk sediment and isolated components (40 mg) were treated with 20 mL of NAPH, PHEN, PYR, or PERY solution (100, 200, 300, 400, and 500 µg L^{-1}) in a background electrolyte solution (pH=7 ± 0.1). The vials were shaken in a thermostated shaking water bath at 200 rpm at 25 ± 2° C for 24 hr (Adeola and Forbes, 2019). Subsequently, supernatants from adsorption experiments were decanted for subsequent measurements, while 20 mL of fresh 0.01 mol L^{-1} $CaCl_2$ containing 200 mg L^{-1} of sodium azide was introduced into the vials containing

the sorbents with 100 to 500 g L^{-1} initial concentration of NAPH, PHEN, PYR or PERY for desorption experiments as previously described (Wang et al., 2008). Prior to the determination of the equilibrium concentration for both adsorption and desorption experiments, the vials were centrifuged at 3000g for 20 min and a 2 mL aliquot of the supernatant was filtered through a 0.45 µm syringe filter. Equilibrium concentrations of NAPH, PHEN, PYR, or PERY were determined by fluorescence spectrophotometry at excitation wavelengths of 280, 290, 341, and 410 nm respectively. The amount of each solute adsorbed and desorbed (q_e, µg g^{-1}) was calculated as follows;

$$q_e = \frac{(C_0 - C_e)V_0}{S_m} \qquad (1)$$

Where C_o (µg L^{-1}) is the initial PAH concentration, C_e (µg L^{-1}) is the equilibrium solute concentration, V_o is the initial volume (L) and S_m is the mass (g) of the adsorbent.

$$\textit{Removal efficiency (\%)} = \frac{(C_0 - C_e)}{C_0} \times 100 \qquad (2)$$

Furthermore, to investigate the competitive or synergistic influence of NOM derived from stream sediments on the removal efficiency of a synthetic graphene-based material (GBM), 20 mg of graphene wool; synthesized via chemical deposition method as previously described (Adeola and Forbes, 2020; Schoonraad et al., 2020), was weighed into 25 pairs of 40 mL amber vials. 10 mg of NAS, MDF, BCF, or MRF were added separately into 5 vials each and 5 vials with graphene wool only were used as a control. 20 mL of PYR solutions (100–500 µg L^{-1}) in 0.01 M $CaCl_2$ background electrolyte solution (pH=7 ± 0.1) were added into the five sets of vials and were equilibrated for 24 hr. All experiments were carried out in triplicate.

2.5. Effect of initial pH and temperature

In this study, the effects adsorption temperature (25, 35, and 45℃) and pH (3, 5, 7, 9, and 11) on the adsorption of NAPH, PHEN, PYR, and PERY onto NAS, MDF, BCF, and MRF were investigated. The pH of the solution was adjusted with 0.1 N HCL and 0.1 N NaOH. Adsorption equilibrium experiments and subsequent quantification were carried out as described in Section 2.4, in triplicate.

2.6. Quality control

Experimental procedures were carried out under strict adherence to quality control guidelines. PAH standards were used to quantify the concentrations of the four PAHs, and the calibration curves showed high correlation coefficients ($R^2 > 0.9$). PAHs were not detectable in blank experiments, which indicated that the influence of pre-existing PAHs in the sediment samples on the overall adsorption was negligible. Each series of experiments was repeated in triplicate to establish reproducibility. For each experiment batch, vials without adsorbent were included as controls. These controls showed no significant losses to the walls of glassware or microbial degradation during the equilibration period.

3.0. Results and Discussion

3.1. Characterization of sorbents

The data on sorbent characterization and PAH properties are presented in Table 1 and S1. The specific surface area (SSA), pore volume, and width were derived from the N_2-BET isotherm; cation exchange capacity (CEC) was calculated from Ca, Mg, K, and Al obtained from ICP-OES (Table S2) (Hendershot and Duquette, 1986), and organic carbon content (% OC) was determined using a thermal combustion method as previously described (Section 2.2). The NOM fractions employed in

this study had varying physical and chemical characteristics and a relatively wide range of organic carbon (OC) content of 3.4 to 9.8 % due to the treatment procedures employed. The point zero net charges shown in Figure S1 revealed that the treatment procedure significantly altered the charge on the surface of the material and PZNC were more acidic (Table 1). The SEM images (Figure 1) reflect the accessibility of the sorbents, as the surfaces were largely heterogeneous, rough, microporous, and had an irregular grain structure with MRF being less aggregated and having a smaller grain size. The treatment procedures created pores with irregular spheres observed in the MDF and BCF sorbent fractions. Optical images revealed different colorations of the bulk sediment and its derivatives.

Table 1: Sorbent fraction characterization

Sorbent	**pH**	**CEC (M_{eq}/100 mg)**	**OC (%)**	**PZNC**	**S_{BET} ($m^2 g^{-1}$)**	**V_{tpv} (cc g^{-1})**	**V_{BET} (nm)**
NAS	6.8	27.4	6.8	5.4	15.3	0.073	7.80
MDF	4.5	1.3	9.4	5.1	26.1	0.145	7.80
BCF	5.7	0.6	9.8	4.4	7.2	0.040	10.68
MRF	6.2	8.4	3.4	2.7	390.5	1.049	7.45

CEC = cation exchange capacity (Hendershot and Duquette, 1986)

OC = organic carbon content (Frangipane et al., 2009, Nelson and Sommers, 2018).

PZNC =point of zero net charge (Mahmood et al., 2011).

S_{BET} = specific surface area by multipoint BET method (Gregg and Sing, 1982)

V_{tpv} = total pore volume calculated from the amount of N_2 adsorbed at P/P_0 = 0.98 (Haghseresht and Lu, 1998).

V_{BET} = BET average pore diameter.

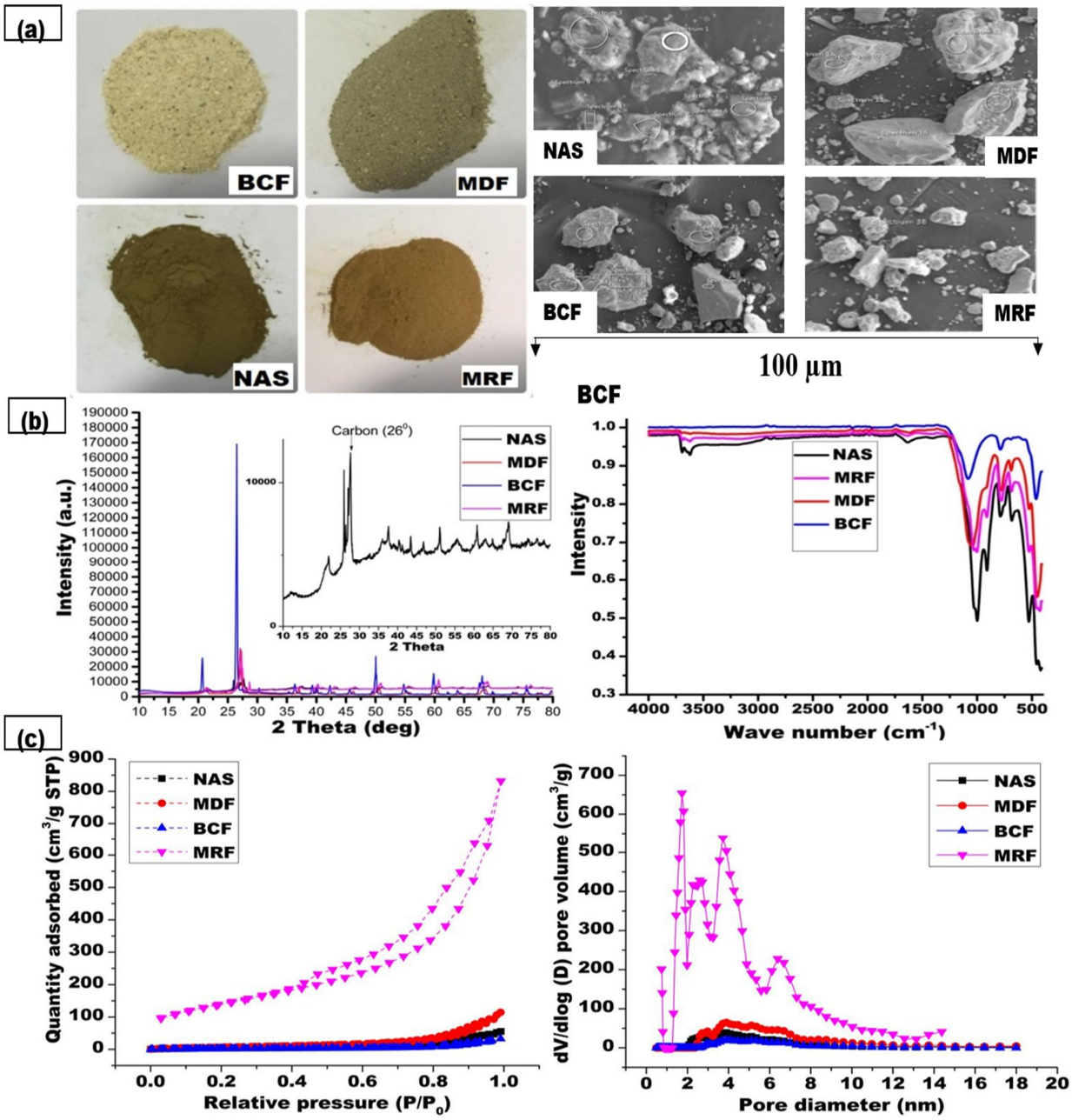

Figure 1: (a) Optical and SEM images (b) XRD and FTIR spectra (c) N_2 – Isotherm and pore size distribution plots for natural sediment and its components.

The hump nature of the XRD pattern (Figure 1) for NAS confirms its amorphous state, whilst the sequential modification thereof led to narrow and sharp peaks, confirming improved crystallinity of

the isolates. The peak at around 26˚ is due to the (002) lattice plane arising from the graphite structure of carbon black, which is more prominent for the BCF fraction with the highest % OC. A slight peak shift to the right for treated samples is due to lattice contraction as a result of the treatment process (Shang et al., 2015). FTIR spectra revealed different intensities of the Fe-O stretching mode (737.3 cm^{-1}) for all samples and a doublet O-H stretching mode associated with $Fe(OH)_2$ and $Fe(OH)_3$ at 3727.9 and 3716.7 cm^{-1} for NAS and MRF samples (Wang and Andrews, 2006). The spectra revealed major adsorption peaks at 1020-1200 cm^{-1}, 1110–1080 cm^{-1}, 400-800 $cm^{-1,}$ and 1650 cm^{-1} assigned to C-OH, siloxane or silicone (Si-O-C), C-O, C=H bends, C-N stretching, and carbonyl (C=O). Generally, the spectra revealed distinct similarities in functionality but different band strengths. The trend in peak intensity of the various sorbents was in the order of BCF < MRF < MDF < NAS. EDS and ICP results (Figure S2 and Table S2) confirmed that the treatment processes altered the mineralogy of the samples, considering the relative abundance of the elements.

Figure 1(c) depicts type-IV N_2 isotherms at standard temperature and pressure (STP), for the sediments and its components derived via the *in-situ* treatment procedure. The plot revealed an H3 hysteresis between the adsorption and desorption isotherms, followed by a steep increase in the amount of N_2-adsorbed at higher relative pressures, previously ascribed to mesoporous adsorbents (Oyedotun et al., 2019), especially the MRF with significantly higher specific surface area (S_{BET}) and pore volume (V_{tpv}) of 390 $m^2\ g^{-1}$ and 1.049 cc g^{-1} respectively (Table 1). Figure 1(c) displays desorption pore size distribution of the sorbents determined via the BJH technique, displaying several peaks which depict that all sorbents possess both microporous (0 – 2 nm) and mesoporous (2 – 8 nm) structures. The SSA and PV were in the order; MRF > MDF > NAS > BCF, interestingly, BCF has the largest pore width of 10.68 nm, which can be attributed to the thermal oxidation (at 375ºC) process that BCF was derived from.

3.2. Sorption kinetics

The pseudo-first-order and pseudo-second-order kinetic models were investigated and compared in order to study the mechanism of the adsorption process (Zhao et al., 2011; Adeola and Forbes, 2020). The amount of solute sorbed per gram of sorbent at equilibrium (q_e) and the first-order and second-order sorption rate constants (k_1 and k_2) can be evaluated from the slope and the intercept deduced from a plot of log ($q_e - q_t$) against t for first-order, and a plot of t/q_t against t for second-order kinetic models, respectively (Lagergren 1898; Younis et al., 2015; Adeola and Forbes, 2019). The kinetic parameters obtained from models employed are summarized in Table 2 and the kinetic plots are displayed in Figure 2. The second-order equation fit far better with experimental data obtained from this study (Figure 2 and S5), with correlation coefficients (R^2) ranging from 0.934 to 0.997, compared with the first-order model with R^2 values ranging from 0.601 to 0.896 (Table 2). The experimental adsorption capacity, q_e, for NAPH, PHEN, PYR, and PERY interaction with different sediment components, is similar to what was calculated or predicted using the second-order kinetic equation, which further confirms that the adsorption process follows the second-order kinetic pathway and this suggests that chemisorption may have occurred either via hydrogen or covalent bonding between the sediment components and the selected PAHs (Yu et al., 2015). The time-concentration profile revealed a fast rate of adsorption occurred in the first 60 min, due to the abundance of sorption sites, before proceeding to equilibrium after different times for the different PAHs and sorbents used in this study (Figure S5).

Table 2: Coefficients of sorption kinetics for adsorption of selected 2- to 5- ringed PAHs by sediment components and the corresponding correlation coefficients (R^2).

PAH	Sorbent	1st Order				2nd Order			
		Cal. q_e ($\mu g\ g^{-1}$)	*Exp.* q_e ($\mu g\ g^{-1}$)	K_1 (min^{-1})	R^2	*Cal.* q_e ($\mu g\ g^{-1}$)	*Exp.* q_e ($\mu g\ g^{-1}$)	K_{2*} (10^{-4}) ($\mu g\ g^{-1} min^{-1}$)	R^2
NAPH	NAS	0.996	894	6.02	0.864	909	894	0.44	0.996
	MDF	0.997	904	4.52	0.658	909	904	3.90	0.997
	BCF	0.995	668	5.76	0.885	667	668	0.58	0.987
	MRF	0.996	778	6.45	0.698	769	778	0.51	0.965
PHEN	NAS	0.997	1089	4.48	0.601	1000	1089	1.09	0.997
	MDF	0.996	1029	3.59	0.678	909	1029	0.83	0.994
	BCF	0.996	832	4.93	0.698	833	832	0.80	0.988
	MRF	0.997	836	4.67	0.729	833	836	1.30	0.991
PYR	NAS	0.996	1005	5.43	0.842	909	1005	1.20	0.985
	MDF	0.995	969	6.18	0.862	833	969	0.45	0.994
	BCF	0.995	405	5.62	0.896	417	405	1.20	0.939
	MRF	0.995	751	5.99	0.885	667	751	0.25	0.934
PERY	NAS	0.995	1261	7.12	0.754	1250	1261	1.31	0.962
	MDF	0.994	2175	7.15	0.878	2000	2175	0.08	0.980
	BCF	0.994	1745	7.85	0.889	1667	1745	1.10	0.980
	MRF	0.996	1560	7.90	0.649	1429	1560	0.36	0.978

Cal. q_e*: Calculated amount adsorbed; Exp.* q_e*: Experimental amount adsorbed;* K_1*: First order rate constant;* K_2*: Second-order rate constant*

Table 2 revealed that *in-situ* mineral enrichment (MRF) which involves the release of minerals trapped in the organic carbon framework and reduction of the % OC content in the sediment sample (Table 1 and S2), led to improved rate constants K_1 and K_2 when compared with NAS. The BCF which is regarded as condensed organic matter due to the extensive cross-linkage which largely defines its structural chemistry (Ran et al., 2002; Ololade et al., 2018), has a lower rate constant K_2 than values obtained for MDF, containing amorphous carbon, for lower molecular weight (LMW) PAHs (NAPH and PHEN). However, the reverse was observed for higher molecular weight (HMW) PAHs (PYR and PERY), with BCF possessing a higher sorption rate constant K_2.

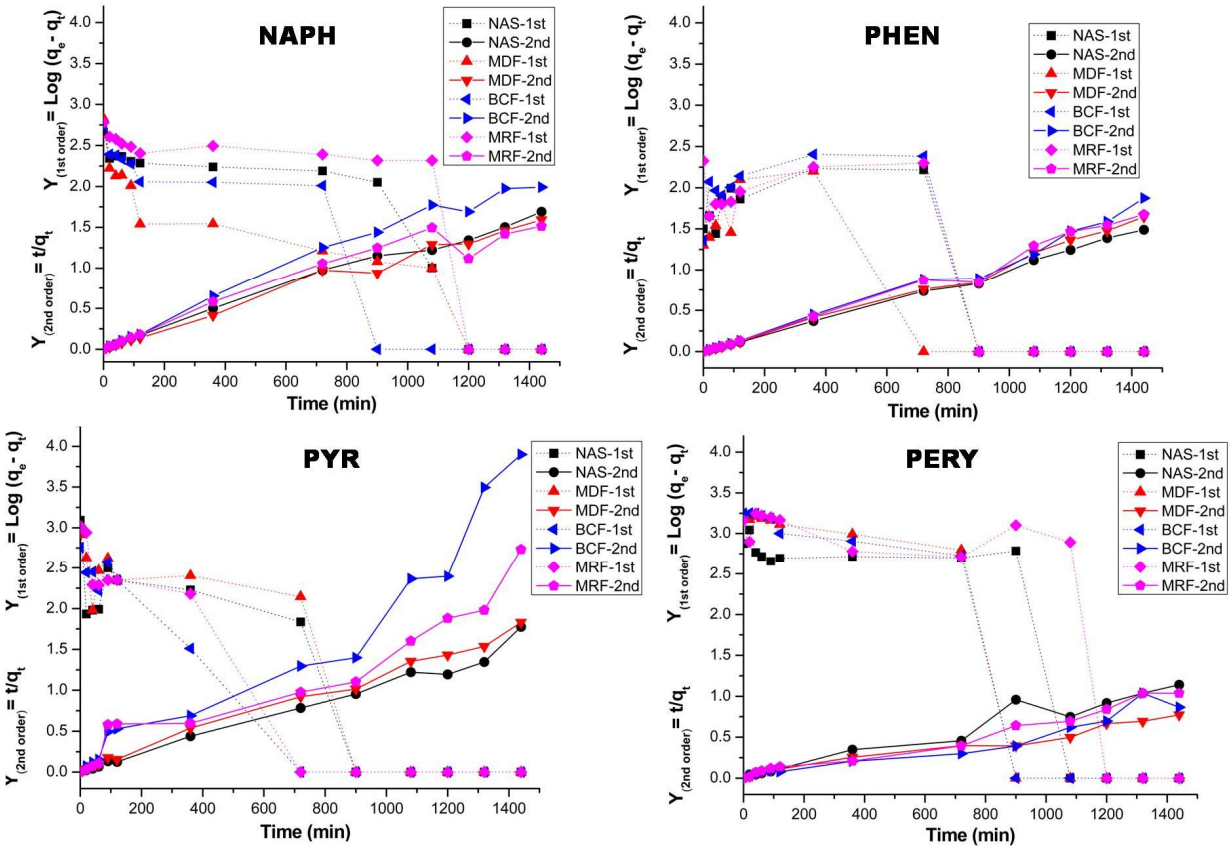

Figure 2: Lagergren pseudo-first-order and pseudo-second-order kinetics sorption for naphthalene, phenanthrene, pyrene, and perylene onto sediment components.

3.3. Sorption isotherm

The characterization results of sorbents revealed both chemical and structural differences (Table 1, Figure S2), and the physicochemical properties of the chosen 2- to 5- membered ring PAHs also vary (Table S1). Hence, differences in the sorption behavior of the four PAHs are expected. The detailed isotherm data are presented in Table S2-S4, a summary of the data is provided in Table 3, and isotherm model plots are presented in Figure S3 and S4. Based on the Error Sum of Squares (SSE) values obtained from nonlinear regression analysis of sorption equilibrium data, complimentary sorption mechanisms took place across all sorbents and PAHs. The results indicate that both multilayer adsorption and partitioning occurred during the sorption experiments, similar to what was reported by Wang et al. (2008). However, the layer-on-layer adsorption mechanism described by the Freundlich model best fits the adsorption data and is validated by the least values of SSE obtained.

The maximum adsorption capacities of sediments were mainly found in the order BCF < MDF < NAS < MRF (Table 3), which correlates with % OC as listed in Table 1. The surface of NOM possesses largely hydrophobic sites that promote hydrophobic-organophilic interactions between the hydrophobic moieties of selected PAHs and sediment components. Table 3 reveals higher values of adsorption capacities (K_f and K_d) and maximum adsorption capacity (q_{max}) for the mineral-deficient fraction (MDF) over the mineral-rich fractions of NOM (MRF), thus establishing a positive correlation between overall adsorption capacities and % OC of the respective fractions.

The adsorption capacity/coefficient (K_d) is also regarded as the partition distribution/partitioning coefficient (K_p) and is derived from the same linear model equation (equation S6). The fact that K_d and/or K_p is lower for higher molecular weight PAHs, suggests that heavier PAHs were less available

for solid-liquid partitioning, unlike lower molecular weight PAHs, This unusual trend may be due to organic vs mineral content of the native sediments and morphology (i.e. pore size and structure) of the sorbents. Results of ICP-OES and EDS analysis revealed that the sediment used in this study is rich in minerals, which could potentially offset the hydrophobicity of the surface of the sorbent and partitioning of HMW PAHs (Yu et al., 2014). However, the relatively higher adsorption maxima (q_{max}) reported for PERY, compared with PYR and PHEN, can be attributed to the fact that sorption mechanisms were not entirely controlled by partitioning but by the tendency for multilayer adsorption of sorbates (Freundlich model).

Several authors have reported that the *N* value relates to the heterogeneity index of the adsorbate and energy distribution of hard, glassy, or condensed natural organic matter. It was also postulated that lower *N* values reflect more heterogeneous adsorption sites and the extent of NOM maturation (Weber et al., 1992; Ran et al., 2002; Ran et al., 2003; Xiao et al., 2004; Ololade et al., 2018). The values of *N* were mostly greater than unity, which affirms that the chemical and thermal treatment procedure led to maturation (irreversible transformation) of the native sediment, making the isolates (MDF and BCF) more organophilic, thus improving their sorption capacities except for MRF. There is stronger interaction between MDF-PAHs and BCF-PAHs, than the interaction between MRF-PAHs, considering the higher values of Langmuir constants, $K_{L,}$ and q_{max} (Table 3). Furthermore, when $N > 1$, as the case for most of the HMW PAHs and NOM used in this study, it depicts an S-type isotherm curve. The S-type shape indicates that there is weak PAH-NOM interaction at lower concentrations and the sorption process is enhanced at higher PAH concentrations (Ololade et al., 2018). However, complete saturation of the NOM was not achieved in this study (Figure S3) in this low concentration range (ppb), as the choice of concentration employed was informed by levels of PAHs typically present in the environment.

Table 3: Summary of Freundlich, Langmuir, and linear sorption parameters for sorption of selected 2- to 5- ringed PAHs onto natural sediment and its component fractions.

Sorption model	Parameter	NAS	MDF	BCF	MRF
	K_f	6.2e-3 - 24.10	9.4e-6 - 70.60	3.1e-2 - 12.36	2.4e-3 - 11.71
Freundlich	N	0.26 - 2.45	0.23 - 3.46	0.04 - 1.85	0.38 - 2.39
	SSE	0.002 - 0.19	0.023 - 2.01	0.200 - 2.24	0.014 - 1.15
Langmuir	q_{max} ($\mu g\ g^{-1}$)	94.1 - 7853.2	54.5 - 10678	239.6 - 13212	234.5 - 5807.4
	K_L ($L\ \mu g^{-1}$)	1.9e-4 - 0.08	2.2e-4 - 0.3	1.5e-4 - 15.30	2e-4 - 0.02
	SSE	0.003 - 0.90	0.069 - 2.60	0.54 - 2.25	0.25 - 1.28
Linear	K_d	0.50 - 6.13	0.32 - 6.05	0.09 - 2.07	0.27 - 3.03
	SSE	0.03 - 1.23	0.19 - 2.60	0.54 - 2.53	0.23 - 1.27
	$LogK_{oc}$	0.85 - 1.34	0.53 - 1.81	0.04 - 1.32	0.60 - 1.93

Freundlich model: $qe=K_fC^Ne$; Langmuir model, $q_e=q_{max}Ce/(K_L+C_e)$; Linear model: $q_e=K_dC_e$; K_{oc} is the OC-normalized sorption capacity coefficient with a unit of $\mu g/g\text{-}OC/(\mu g\ L^{-1})^n$.

3.4. Desorption isotherms and hysteresis effects

Desorption experiments were conducted using the adsorbed PAHs on each NOM sample as the total mass of sorbate in the desorption system and the actual amount desorbed was accounted for with the aid of the mass balance equation (*Eq. 1*). This was necessary to be able to predict the release potential, binding capacities, and risk of environmental recontamination associated with adsorbed PAHs (Wang et al., 2008).

Table 4 revealed that there was a significant difference between the adsorption intensity (N_{ads}) and desorption intensity (N_{des}). Therefore, the hysteresis indices *(H) (H* = N_{ads}/N_{des}*)*, for the PAHs across the different NOM were greater than 1 for HMW PAHs (PYR & PERY), which suggests that sorption–desorption hysteresis took place to a larger extent. However, NAPH and PHEN displayed some degree reversible adsorption onto different NOMs, with *H*-indices less than 1. The unique behavior of NAPH and PHEN can be attributed to its physicochemical properties, such as lower molecular weight and hydrophobicity (Log*Kow*) (Table S1). It is worthy to note that the majority of the *H*-indices for PAHs were in the order, PERY > PYR > PHEN > NAPH, which reflect differences in binding strengths, while *in-situ* sediment treatment led to greater desorption of adsorbed PAHs, as % desorption values were higher in modified NOM than untreated sediments, thus revealing that the isolates had a lower capacity to retain PAHs. Table 4 revealed that the native (NAS) sample had the least % desorption across the PAHs investigated, which may be due to its pristine condition and high binding strength (q_{max}). The relatively high % desorption of MRF reflects its inability to retain PAHs, due to its morphology and/or low % OC content. Higher % desorption for larger PAHs (PYR and PERY) as compared to smaller PAHs can be attributed to size-controlled interactions between sorbate molecules and active sites/pores. Smaller PAHs are expected to penetrate deeper into pores via intra-particle diffusion and are thus more difficult to remove (Hall et al., 2009). Adsorption and desorption are complementary processes that take place simultaneously at different rates during batch sorption experiments until the maximum adsorption capacity of the material is reached. Hysteresis, which is regarded as irreversible adsorption, occurs when the intensity (N_{ads}) of adsorption is greater than desorption intensity (N_{des}) (Cornelissen et al., 2005).

Table 4: Sorption-desorption parameters and hysteresis indices derived from the Freundlich isotherm model

PAH	Sorbent	$LogK_{f\ (des)}$	N_{ads}	N_{des}	$^{*}H$	Desorption ± SD (%)
NAPH	NAS	1.82	0.89	2.87	0.31	6.19 ± 5.65
	MDF	1.79	1.19	3.24	0.37	8.23 ± 6.29
	BCF	1.17	1.32	1.69	0.78	12.49 ± 6.57
	MRF	1.62	0.59	2.94	0.20	8.97 ± 6.98
PHEN	NAS	1.33	0.26	2.27	0.12	10.02 ± 3.62
	MDF	0.92	0.31	1.29	0.24	17.92 ± 17.60
	BCF	-0.78	0.04	0.39	0.10	27.72 ± 36.24
	MRF	3.86	1.15	0.54	2.13	35.87 ± 33.74
PYR	NAS	0.82	0.79	0.47	1.68	54.52 ± 16.61
	MDF	2.21	4.24	4.16	1.02	62.67 ± 14.44
	BCF	-0.56	1.46	1.19	1.23	86.38 ± 17.67
	MRF	-12.21	0.38	0.17	2.23	70.18 ± 17.96
PERY	NAS	4.86	2.45	1.22	2.01	53.49 ± 7.96
	MDF	-14.78	2.57	0.15	17.13	67.53 ± 11.84
	BCF	0.55	1.85	0.76	2.43	54.44 ± 6.04
	MRF	3.17	2.39	0.28	8.54	63.17 ± 13.74

**H: Sorption-desorption hysteresis index, $H = N_{ads}/N_{des}$; SD: Standard deviation*

For a material designed for remediation, it is preferred that the *H* index be greater than 1 in an aqueous medium, which reflects higher adsorption intensity and lower desorption intensity. Thus the employment of a suitable organic solvent would be required to force or enhance desorption/regeneration after the adsorption cleanup has been achieved. An *H*-index greater than unity is also desirous in aquatic environments as adsorbed organic contaminants (OCs) held by sediments will pose a lower tendency to recontaminate surface water. Adsorbent pore deformation (irreversible collapse or disorientation) and hydrophobicity of the sorbates are responsible for

hysteretic behavior in sorption dynamics (Lu and Pignatello, 2002). PAH-induced alteration of the sorbent and solution chemistry (Adeola and Forbes, 2020), were potential factors that could lead to the build-up of pressure, pore expansion, pore deformation, and deviation of NOM from the native thermodynamic state.

3.5. Effect of pH on the sorption of PAHs onto sediment components

Solution pH influences the sorption process of many organic contaminants onto different soils and sediments because it alters the net charge of the adsorbent and sorbate (Ololade et al., 2018; Adeola and Forbes, 2020). Several reports indicate that PAH sorption is not influenced by pH since PAHs do not ionize in water (Guo et al., 2018). However, depending on the nature of the adsorbent, solution pH may influence the sorption process of PAHs (Huang et al., 1996).

Generally, acidic pH appears to favor adsorption of the PAHs slightly more than basic pH across the NOM fractions and the role of pH was more significant for perylene (PERY) adsorption (Figure 3). The PZNC of the sorbents ranged from 2.7 to 5.4 (Table 1, Figure S1). Thus, the somewhat higher % adsorption of the respective PAHs onto the different sediment components under acidic conditions may be as a result of the positively charged surface of the adsorbent in acidic solution, which may promote the formation of hydrogen bonds and/or electrostatic attraction between the PAHs and sediment components due to the presence of -NH, C-OH and -OH groups in the sediment components. It is noteworthy that the effect of pH on adsorption of any of the 5-ringed PAHs onto any material at all has only been reported once in the literature (Schlautman and Morgan, 1994). Schlautman and Morgan (1994) reported that samples containing minerals such as silicates, as we have in NOM fractions (Table S2), have point zero surface charge at pH $\geq$ 2.0. Point zero charge (PZC or PZNC) is the point in which the net surface charge of the material is zero, and this could be

anywhere on the pH scale for different materials (Bakatula et al 2018). For the materials described by Schlautman and Morgan (1994), the surface of the material is dominantly negatively charged at pH>2, leading to electrostatic repulsion and a decline in % adsorption occurs.

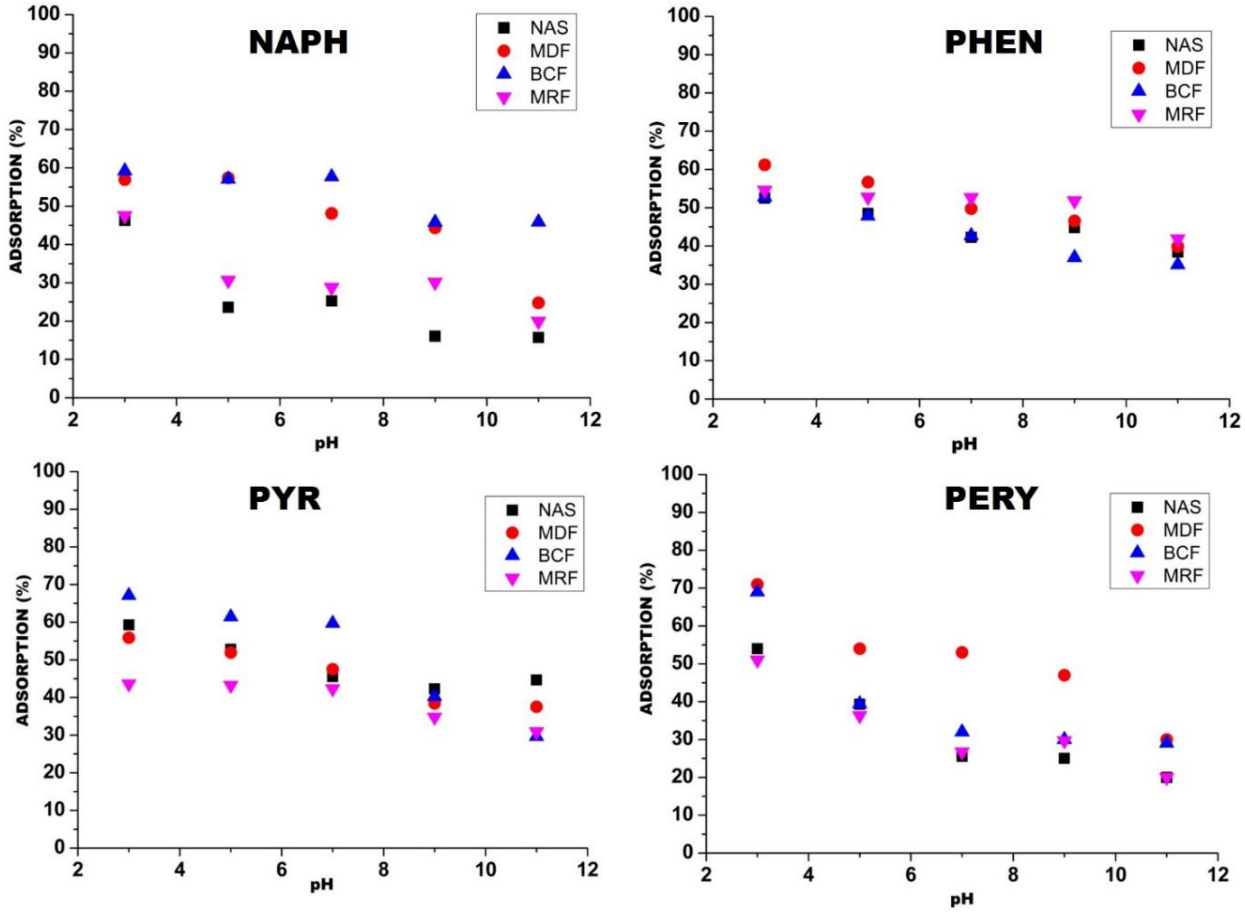

Figure 3: Effect of solution pH on adsorption of selected PAHs onto sediment components. (Experimental conditions: C_o = 500 µg L^{-1}; dosage = 1 g L^{-1}, mixing rate = 200 rpm, T = 25 ± 1 °C, contact time: 24 hr).

3.6. Effect of temperature and thermodynamic studies

Thermodynamic parameters such as Gibb's free energy (ΔG), enthalpy (ΔH), and entropy (ΔS) of the adsorption process for PAH and NOM were estimated from the Vant't Hoff plots (Figure 4), using the Van't Hoff equations (*Eq.* 3 and 4) (Yakout and Daifullah, 2013; Gupta and Singh, 2018; Adeola and Forbes, 2019)

$$ln\, K_d = \frac{\Delta S^\circ}{R} - \frac{\Delta H^\circ}{RT} \quad (3)$$

$$\Delta G^\circ = \Delta H^\circ - T\Delta S^\circ \quad (4)$$

1

Temperature plays a significant role in several chemical and physical processes as some reactions are feasible at room temperature, while others require an additional supply of heat energy to initiate the reaction. Therefore, the role of temperature on the adsorption of NAPH, PHEN, PYR, and PERY onto sediment components was studied at 298, 308, and 318 K, respectively.

The Van't Hoff plot (Figure 4) revealed that the adsorption capacity of the different NOM fractions, expressed as "$ln\, K_d$", increased with an increase in temperature for the LMW PAHs (NAPH & PHEN), but decreased for HMW PAHs (PYR & PERY). Table S7 also revealed that adsorption of the PAHs onto the stream sediment components involved a spontaneous endothermic reaction for LMW PAHs (NAPH & PHEN), with positive and negative values of ΔH and ΔG respectively. For the HMW PAHs used in this study, heat is generated and emitted to the surroundings, indicating an exothermic process with negative enthalpy values (-ΔH) for PYR and PERY. Furthermore, an increase in temperature improves the sorption feasibility for NAPH and PHEN as ΔG became more negative, whilst for PYR and PERY adsorption was more feasible at room temperature or below, considering the trend in ΔG values. Several reports have shown that the thermodynamic behavior of PAHs differs for different adsorbents (Ghosh et al., 2001; Zhao et al., 2011; Younis et al., 2015; El-shahawi et al., 2017; Gupta and Singh, 2018).

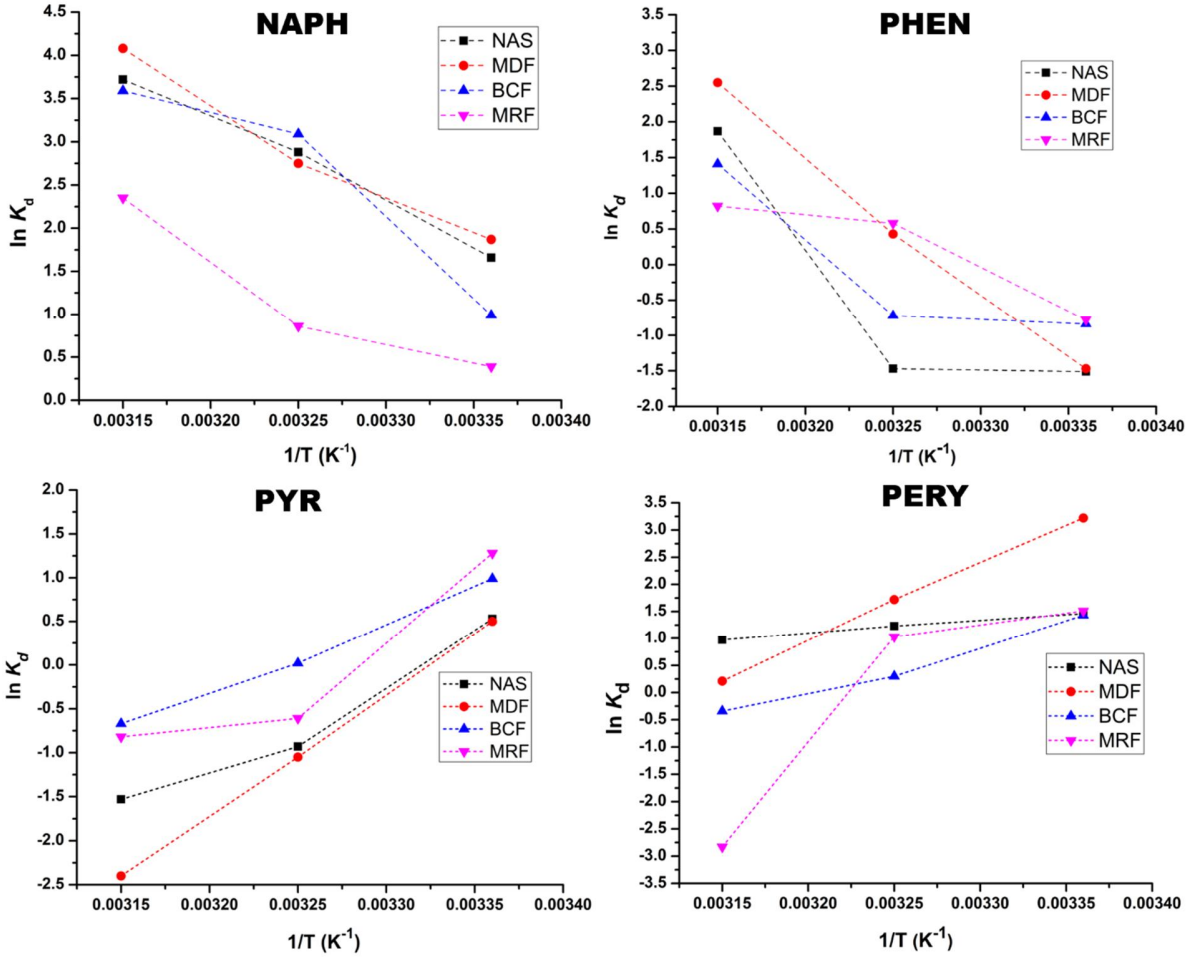

Figure 4: Plot of Van't Hoff plots for NAPH, PHEN, PYR and PERY adsorption onto sediment components at 298, 308 and 318 K.

Some sorbate-sorbent interactions are endothermic, such as pyrene adsorption by some carbonaceous adsorbents (Younis et al, 2015, Girardello et al., 2016 Adeola and Forbes, 2019), while pyrene interaction with activated carbon and mineral-rich geosorbents has been reported to be exothermic (El-shahawi et al., 2017; Hassan et al., 2018). Furthermore, both positive and negative values of ΔH within the range of -7,100 J mol^{-1} and + 3,800 J mol^{-1} were reported for NAPH sorption onto silt under different temperature regimes, suggesting that both endothermic and exothermic

sorption processes may occur within the same sorbate-sorbent interaction (Wauchope et al., 1983, Unuabonah et al., 2016). This further confirms the complex sorption thermodynamics of PAHs and affirms the importance of temperature regimes in the adsorption process towards its application in the remediation of PAH pollution. Thermodynamic parameters are influenced by the morphology and chemical composition of the NOM fractions, which vary for different geological environments, and thus the sequestration of different PAHs within sediments in an ecological environment cannot be fully understood if the composition of the NOM is not determined.

3.7. Influence of NOM on GW-pyrene interaction

A detailed study on the adsorption kinetics and sorption-desorption isotherm of pyrene interaction with graphene wool (GW) has previously been reported (Adeola and Forbes, 2019). Thus, this section focuses on results obtained from the addition of different NOM fractions into solutions containing graphene wool and pyrene, in order to establish the synergistic or competitive influence of sediment components on the overall removal efficiency of pyrene by graphene wool (GW). Table 5 and Figure 5 revealed that the presence of the sediment components/NOM in the sorption process played a dominant competitive role and had an inhibitory effect on the overall removal efficiency of pyrene. The presence of NOM altered the sorption mechanism from multilayer adsorption, described by the Freundlich isotherm model for GW-pyrene, to a monolayer adsorption mechanism for GW-NOM-pyrene interactions; considering the R^2 values (Table 1). Furthermore, the influence of bulk sediment and its components differ as removal efficiencies were in the order of GW > GW-BCF > GW-NAS > GW-MDF > GW-MRF (Figure 5). The high maximum adsorption capacity (q_{max}) of GW-BCF (Table 5), suggests that the presence of condensed organic carbon (BCF) in a PAH contaminated water body would potentially be least detrimental to the removal efficiency of GBMs. MRF significantly impeded

the removal of pyrene from aqueous solution as adsorption capacity (K_d), experimental amount adsorbed (*Exp.* q_e), and removal efficiency reduced (16.9 to 0.3 g L^{-1}), (230.8 to 43.2 µg g^{-1}) and (95.4 to 16.5 %) respectively. This suggests that the presence of NOM containing high amounts of minerals may reduce the adsorption efficiency of graphene wool significantly, as the minerals could be leached into the solution and adversely alter the solution's chemistry (Lamichhane et al., 2016).

There are reports that metals and other minerals bind strongly to graphene-based materials (GBMs) (Xu and Wang, 2017). Therefore, it can be hypothesized that the prominent inhibitory role of MRF maybe because some of the minerals listed in Table S2, may have leached into the solution and competitively adsorbed on the sorption sites of GW due to the comparatively larger surface area of MRF (BET-Figure 1(c) and Table 1), or that NOM rich with minerals will possess a strong affinity for graphene active sites, thus clogging and reducing the number of available sites (resulting in them being less organophilic) for pyrene adsorption onto GW. Cai et al. (2015) reported that NOM is sorbed rapidly by graphene, which diminishes the available sites for PAH adsorption. However, we have been able to further relate that NOM with high OC content, would compete for sites with PAHs, but still allows for some degree of PAH adsorption as compared to NOM rich in minerals.

Table 5: Freundlich, Langmuir and linear sorption parameters for sorption of pyrene onto GW and GW-NOM hybrids.

Sorption model	Parameter	GW	GW-NAS	GW-MDF	GW-BCF	GW-MRF
	$LogK_f$	1.89	-3.87	-0.79	0.46	-0.13
Freundlich	N	3.2	0.2	0.8	1.1	5.2
	R^2	0.999	0.946	0.993	0.993	0.899
Langmuir	q_{max} ($\mu g\ g^{-1}$)	344.8	35.6	212.8	1667.0	23.2
	K_L ($L\ \mu g^{-1}$)	0.1	0.009	0.002	0.001	0.002
	R^2	0.996	0.953	0.995	0.997	0.979
Linear	K_d ($g\ L^{-1}$)	16.9	4.2	0.6	1.8	0.3
	Exp. q_e ($\mu g\ g^{-1}$)	230.8	128.2	81.7	138.1	43.2
	R^2	0.940	0.948	0.985	0.985	0.706
	RE (%)	95.8	67.4	38.0	75.1	16.5

Freundlich model: $q_e = K_f C^N e$; Langmuir model, $q_e = q_{max} Ce/(K_L + C_e)$; Linear model: $q_e = K_d C_e$; Exp. q_e: Experimental amount adsorbed. RE (%): percent removal efficiency

It is also noteworthy that the conductivity of the solution containing 20 mg GW and pyrene decreased on the addition of 10 mg of different NOM, from 828 µS cm^{-1} (GW) to 815 µS cm^{-1} (GW-NAS), 810 µS cm^{-1} (GW-MDF), 822 µS cm^{-1} (GW-BCF) and 789 µS cm^{-1} (GW-MRF). An increase in pH was also observed: from an acidic pH of 6.48 to a basic pH of 7.23 for GW and GW-MRF in pyrene contaminated solutions, while GW-NAS, GW-MDF, and GW-BCF maintained fairly acidic with pHs of 6.85, 6.52, and 6.59 respectively. These changes in solution chemistry may play a vital role in pyrene adsorption by graphene wool and other GBMs, especially regarding ionic strength and pH. An increase in solutions' ionic strength and an acidic pH has been reported to enhance the adsorption of pyrene by GBMs (Lamichhane et al., 2016; Adeola and Forbes, 2019). Thus, the inhibitory influence of sediment components can be attributed to the unfavorable conditions created by the NOMs, especially by the presence of mineral-rich NOM fractions which could lead to fouling of graphene wool, if utilized for water treatment application.

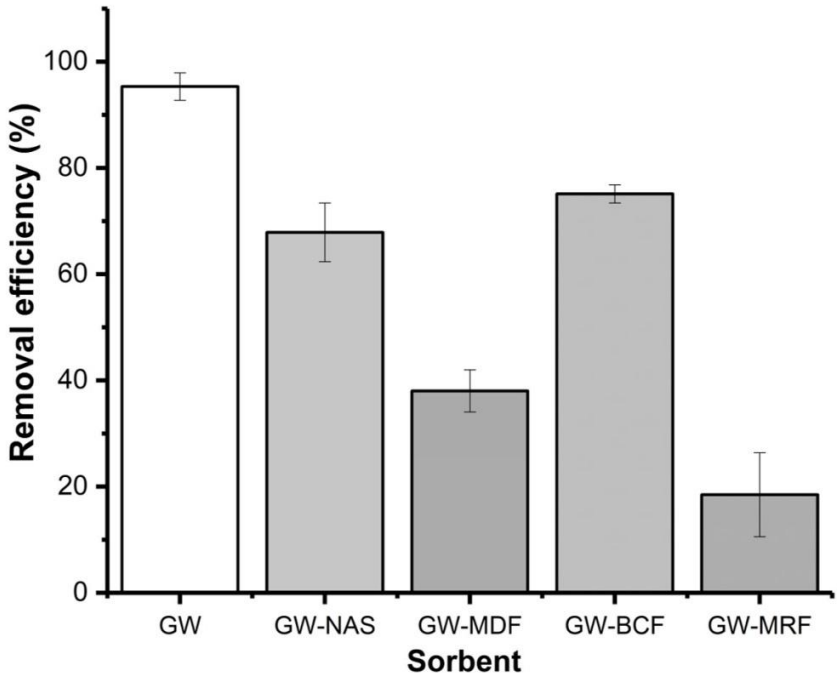

Figure 5: Removal efficiency and adsorption capacity (K_d) of pyrene by graphene wool (GW) in the presence of different NOM.

3.8. Influence of the number of aromatic rings on sorption capacity

Several reports indicate that PAHs interact with different carbonaceous adsorbents mainly via π-π interactions (Amstaetter et al., 2012; Wang et al., 2014; Nsibande et al., 2019; Adeola and Forbes, 2019). The number of aromatic rings is directly proportional to the number of π- electrons available for bonding, thus the experimental amount adsorbed of the selected PAHs for sediment components was mainly in the order of PERY > PYR > PHEN > NAPH (Figure S5).

Generally, oxides of metals in high oxidation states, such as Fe^{3+} and Al^{3+}, are Lewis acids that can act as electron-withdrawing species due to their vacant orbitals, which could potentially displace hydrogen from aromatic rings in solution, thereby causing the weakening or deactivation of the aromatic ring (Kuznetsov et al., 2018). Therefore, in the quest to stabilize the aromatic rings, delocalized π-electrons that could have been available for bonding, are held by PAHs to strengthen the rings. The electron-withdrawing nucleophilic atoms present in relatively high concentration in the mineral-rich fraction of the sediment components (Table S2), may be responsible for why MRF has a lower adsorption intensity (K_L) than MDF across most of the PAHs (Table 3), and the significant inhibitory influence played by MRF on sorption efficiency of GW (Figure 5).

On the contrary, the higher values of % OC for BCF and MDF enhance their hydrophobic nature due to the high degree of aliphatic and aromatic compounds they possess (Ran et al., 2007). Furthermore, aromaticity contributes largely to octanol-water partition coefficients (K_{ow}) of organic contaminants, as K_{ow} is used to describe the extent of hydrophobicity of compounds. Thus, improved sorptive interaction between NOMs (BCF and MDF) and PAHs can be attributed to the relative abundance of hydrophobic aromatic moieties, and hydrophobic interactions between PAHs and hydrophobic moieties of the NOM contributed extensively to the overall hydrophobic-organophilic sorption process.

4.0. Conclusion

The *in-situ* modification of natural organic matter derived from stream sediment was used to establish the roles of different fractions of NOM on the sequestration of selected PAHs via a sorption process. Delineation of sediment components was achieved via effective chemical and thermal treatment procedures, confirmed by XRD, SEM-EDX, ICP-OES, FTIR, BET as well as other basic characterization to determine % organic carbon (OC), sorbent pH, etc. Results suggest that *in-situ* removal of various NOM components has a significant influence on the adsorption-desorption potential of PAHs. MDF and BCF fractions adsorbed PAHs to a greater extent than mineral-rich fractions. Furthermore, the sorption process of selected PAHs onto all sorbent fractions was dominated by the interaction between hydrophobic moieties and hydrophobic sites at the sediment-water boundary/interface rather than by the surface area of sorbents. The observed hysteresis revealed the potential impact of each sediment component on the sequestration of PAHs in aquatic systems. With respect to the recontamination of surface water, NOMs with higher % OC would bind PAHs more and would not readily desorb them at the same intensity with which they were adsorbed (hysteresis), thus making PAHs more persistent in sediments and less bioavailable in water.

Graphene-based materials (GBMs) have attracted significant interest for water treatment applications in the last two decades. Therefore, the influence of NOM on the efficiency of these materials in the treatment of PAH-contaminated water provides useful information, as NOM is present in aquatic systems as dissolved organic carbon (DOC) and particulate organic carbon (POC). Results revealed that the presence of NOM diminishes the efficiency of the adsorption of pyrene by graphene wool by altering the solution chemistry, clogging sorption sites, and/or selectively binding to active sites, with the mineral-rich fraction (MRF) of NOM impeding the adsorption of PAHs the most. This study revealed the invaluable role of black carbon (BC) and amorphous carbon, as well as mineral

enrichment, in the adsorption and retention of hydrophobic organic compounds (HOCs) within sediment matrices, and the potential impact of each NOM fraction in the environmental risk management (remediation) of PAH contaminated water.

Acknowledgments

Authors acknowledge the University of Pretoria Commonwealth Doctoral Scholarship funding (AA), Rand Water, and the Departments of Chemistry and Physics at the University of Pretoria, South Africa for their support.

Conflict of interest

The authors declare that there is no conflict of interest regarding the publication of this article.

References

Adeola, A.O., Forbes, P.B.C., 2020. Optimisation of the sorption of selected polycyclic aromatic hydrocarbons by regenerable graphene wool. Water Sci. Technol. 80(10), 1931-1943. doi: https://doi.org/10.2166/wst.2020.011.

Adeniji, A.O., Okoh, O.O., Okoh, A.I. 2019. Levels of polycyclic aromatic hydrocarbons in the water and sediment of Buffalo River Estuary, South Africa and their health risk assessment. Arch. Environ. Contam. Toxicol. 76, 657–669. https://doi.org/10.1007/s00244-019-00617-w

Amstaetter, K., Eek, E., Cornelissen, G., 2012. Sorption of PAHs and PCBs to activated carbon: Coal versus biomass-based quality. Chemosphere 87, 573-578. https://doi.org/10.1016/j.chemosphere.2012.01.007.

Bakatula, E.N., Richard, D., Neculita, C.M., Zagury, G. J. 2018. Determination of point of zero charge of natural organic materials. Environ. Sci. Pollut. Res. 25, 7823–7833. https://doi.org/10.1007/s11356-017-1115-7

Cornelissen, G., Gustafsson, Ö., Bucheli, T.D., Jonker, M.T.O., Koelmans, A.A., van Noort, P.C.M., 2005. Extensive sorption of organic compounds to black carbon, coal, and kerogen in sediments

and soils: mechanisms and consequences for distribution, bioaccumulation, and biodegradation. Environ. Sci. Technol. 39, 6881-6895. https://doi.org/10.1021/es050191b.

Crisafully, R., Milhome, M.A., Cavalcante, R.M., Silveira, E.R., De Keukeleire, D., Nascimento, R.F., 2008. Removal of some polycyclic aromatic hydrocarbons from petrochemical wastewater using low-cost adsorbents of natural origin. Bioresour. Technol. 99, 4515-4519. https://doi.org/10.1016/j.biortech.2007.08.041

El-shahawi, M., Bashammakh, A. S., Alwael, H., Alsibaai, A. A., Dowaidar, A. M. 2017. Adsorption characteristics of polycyclic aromatic hydrocarbons from non-aqueous media using activated carbon derived from phenol formaldehyde resin: Kinetics and thermodynamic study. Environ. Sci. Poll. Res. Int. 24(5), 4228-4240. https://doi.org/10.1007/s11356-015-4936-2

Das, L., Das, P., Bhowal, A., Bhattachariee, C. 2020. Synthesis of hybrid hydrogel nano-polymer composite using Graphene oxide, Chitosan and PVA and its application in waste water treatment. Environ. Technol. Innov. 18, 100664. doi:https://doi.org/10.1016/j.eti.2020.100664

Frangipane, G., Pistolato, M., Molinaroli, E., Guerzoni, S., Tagliapietra, D. 2009. Comparison of loss on ignition and thermal analysis stepwise methods for determination of sedimentary organic matter. Aquat. Conserv. 19, 24-33. https://doi.org/10.1002/aqc.970

Gelinas, Y., Prentice, K.M., Baldock, J.A., Hedges, J., 2001. An improved thermal oxidation method for the quantification of soot/graphite carbon in sediments and soils. Environ. Sci. Technol. 21, 3519–3525. https://doi.org/10.1021/es010504c.

Girardello, F., Rovani, S., Giovanela, M., Fernandes, A. N. 2016. Removal of pyrene from aqueous solutions by adsorption onto Brazilian peat samples. Adsorpt. Sci. Technol. 34, 538-551. https://doi.org/10.1177%2F0263617416670168

Ghosh, U., Talley, J.W., Luthy, R.G., 2001. Particle-Scale Investigation of PAH Desorption Kinetics and Thermodynamics from Sediment. Environ. Sci. Technol. 35, 3468-3475. https://doi.org/10.1021/es0105820.

Gregg, S., Sing, K. 1982. Adsorption, surface area and porosity. 2nd ed. Academic Press.

Guo, W., Wang, S., Wang, Y., Lu, S., Gao, Y., 2018. Sorptive removal of phenanthrene from aqueous solutions using magnetic and non-magnetic rice husk-derived biochars. R. Soc. Open Sci. 5, 172382-172382. https://doi.org/10.1098/rsos.172382.

Gupta, H., Kumar, R. 2020. Distribution of selected polycyclic aromatic hydrocarbons in urban soils of Delhi, India. Environ. Technol. Innov. 17, 100500. https://doi.org/10.1016/j.eti.2019.100500

Gupta, H., Singh, S. 2018. Kinetics and thermodynamics of phenanthrene adsorption from water on orange rind activated carbon. Environ. Technol. Innov. 10, 208-214. doi:https://doi.org/10.1016/j.eti.2018.03.001

Haghseresht, H., Lu, G. 1998. Adsorption characteristics of phenolic compounds onto coal-rejected-derived adsorbents. Energ. Fuels. 12:1100-11007. https://doi.org/10.1021/ef9801165

Hendershot, W.H., Duquette, M. 1986. A simple barium chloride method for determining cation exchange capacity and exchangeable cations. Soil. Sci. Soc. 15, 178-191. https://doi.org/10.2136/sssaj1986.03615995005000030013x

Hall, S., Tang, R., Baeyens, J., Dewil, R., 2009. Removing polycyclic aromatic hydrocarbons from water by adsorption on silicagel. Polycycl. Aromat. Comp. 29, 160-183. https://doi.org/10.1080/10406630903017534

Hiller, E., Jurkovič, L., BartaĽ, M., 2008. Effect of temperature on the distribution of polycyclic aromatic hydrocarbons in soil and sediment. Soil & Water Res. 4, 231–240. https://doi.org/10.17221/28/2008-SWR

Hong, L., Ghosh, U., Mahajan, T., Zare, R.N., Luthy, R.G., 2003. PAH sorption mechanism and partitioning behavior in lampblack-impacted soils from former oil-gas plant sites. Environ. Sci. Technol. 37, 3625-3634. https://doi.org/10.1021/es0262683.

Huang, W., Schlautman, M.A., Weber, W.J., 1996. A distributed reactivity model for sorption by soils and sediments. 5. The influence of near-surface characteristics in mineral domains. Environ. Sci. Technol. 30, 2993-3000. https://doi.org/10.1021/es960029w.

Karickhoff, S.W., Brown, D.S., Scott, T.A., 1979. Sorption of hydrophobic pollutants on natural sediments. Water Res. 13, 241-248. https://doi.org/10.1016/0043-1354(79)90201-X

Kraaij, R., Mayer, P., Busser, F.J.M., van het Bolscher, M., Seinen, W., Tolls, J., Belfroid, A.C., 2003. Measured pore-water concentrations make equilibrium partitioning work a data analysis. Environ. Sci. Technol. 37, 268-274. https://doi.org/10.1021/es020116q.

Kuznetsov, D.A., Han, B., Yu, Y., Rao, R.R., Hwang, J., Román-Leshkov, Y., Shao-Horn, Y., 2018. Tuning Redox Transitions via Inductive Effect in metal oxides and complexes, and implications in oxygen electrocatalysis. Joule 2, 225-244. https://doi.org/10.1016/j.joule.2017.11.014.

Lamichhane, S., Bal Krishna, K.C., Sarukkalige, R., 2016. Polycyclic aromatic hydrocarbons (PAHs) removal by sorption: A review. Chemosphere 148, 336-353. https://doi.org/10.1016/j.chemosphere.2016.01.036.

Lagergren, S., 1898. About the theory of so-called adsorption of soluble substances. Kungliga Svenska Veteskapsakademiens Handlingar, Band 24, 1-29.

Loonen, H., Tonkes, M., Parsons, J.R., Govers, H.A.J., 1994. Bioconcentration of polychlorinated dibenzo-p-dioxins and polychlorinated dibenzofurans in guppies after aqueous exposure to a complex PCDD/PCDF mixture: relationship with molecular structure. Aquat. Toxicol. 30, 153-169. https://doi.org/10.1016/0166-445X(94)90011-6.

Lu, Y., Pignatello, J.J., 2002. Demonstration of the “Conditioning Effect” in Soil Organic Matter in Support of a Pore Deformation Mechanism for Sorption Hysteresis. Environ. Sci. Technol. 36, 4553-4561. https://doi.org/10.1021/es020554x.

Mikutta, R., Kleber, M., Kaiser, K., Jahn, R., 2005. Review: Organic matter removal from soils using hydrogen peroxide, sodium hypochlorite, and disodium peroxodisulfate. Soil Sci. Soc. Am. J. 69, 129-135. https://doi.org/10.2136/sssaj2005.0120

Nelson, D.W., Sommers, L.E. 2018. Total carbon, organic carbon, and organic matter. In methods of soil analysis (eds D. Sparks, A. Page, P. Helmke, R. Loeppert, P.N. Soltanpour, M.A. Tabatabai, C.T. Johnston and M.E. Sumner). https://doi.org/10.2136/sssabookser5.3.c34.

Nsibande, S. A., Montaseri, H., Forbes, P. B. C. 2019. Advances in the application of nanomaterial-based sensors for detection of polycyclic aromatic hydrocarbons in aquatic systems. TRAC-Trend Anal. Chem., 115, 52-69. https://doi.org/10.1016/j.trac.2019.03.029

Mahato, J. K., Gupta, S. K. 2020. Modification of Bael fruit shell and its application towards natural organic matter removal with special reference to predictive modeling and control of THMs in drinking water supplies. Environ. Technol. Innov. 18, 100666. https://doi.org/10.1016/j.eti.2020.100666

Mahmood, T., Saddique, M.T., Naeem, A., Westerhoff, P., Mustafa, S., Alum, A. 2011. Comparison of different methods for the point of zero charge determination of NiO. Ind. Eng. Chem. Res. 50, 10017–10023. https://doi.org/10.1021/ie200271d

Mojiri, A., Zhou, J. L., Ohashi, A., Ozaki, N., Kindaichi, T. 2019. Comprehensive review of polycyclic aromatic hydrocarbons in water sources, their effects and treatments. Sci. Total Environ. 696, 133971. https://doi.org/10.1016/j.scitotenv.2019.133971

Okoli, C. P., Adewuyi, G. O., Zhang, Q., Zhu, G., Wang, C. Guo, Q. 2015. Aqueous scavenging of polycyclic aromatic hydrocarbons using epichlorohydrin, 1,6-hexamethylene diisocyanate and 4,4-methylene diphenyl diisocyanate modified starch: Pollution remediation approach. Arabian J. Chem. 12(8), 2760-2773. https://doi.org/10.1016/j.arabjc.2015.06.004

Ololade, I.A., Adeola, A.O., Oladoja, N.A., Ololade, O.O., Nwaolisa, S.U., Alabi, A.B., Ogungbe, I.V., 2018. In-situ modification of soil organic matter towards adsorption and desorption of phenol and its chlorinated derivatives. J. Environ. Chem. Eng. 6, 3485-3494. https://doi.org/10.1016/j.jece.2018.05.034.

Opdyke, D.R., Loehr, R.C., 1999. Determination of Chemical Release Rates from Soils: Experimental Design. Environ. Sci. Technol. 33, 1193-1199. https://doi.org/10.1021/es9806074.

Oyedotun, K. O., Masikhwa, T. M., Lindberg, S., Matic, A., Johansson, P., Manyala, N. 2019. Comparison of ionic liquid electrolyte to aqueous electrolytes on carbon nanofibres supercapacitor electrode derived from oxygen-functionalized graphene. Chem. Eng. J. 375, 121906. https://doi.org/10.1016/j.cej.2019.121906

Ran, Y., Huang, W., Rao, P.S.C., Liu, D., Sheng, G., Fu, J., 2002. The Role of Condensed Organic matter in the nonlinear sorption of hydrophobic Organic contaminants by a peat and sediments. J. Environ. Qual. 31, 1953-1962. https://doi.org/10.2134/jeq2002.1953

Ran, Y., Sun, K., Ma, X., Wang, G.H., Grathwohl, P., Zeng, E.Y., 2007. Effect of condensed organic matters on solvent extraction and aqueous leaching of PAHs based in soils and sediments. J. Environ. Pollut. 43, 111–123. https://doi.org/10.1016/j.envpol.2006.11.028.

Ran, Y., Xiao, B., Huang, W., Peng, P., Liu, D., Fu, J., Sheng, G., 2003. Kerogen in an aquifer and its strong sorption for hydrophobic organic contaminants. J. Environ. Qual. 32(5):1701-1709. https://doi.org/10.2134/jeq2003.1701.

Schlautman, M.A., Morgan, J.J., 1994. Sorption of Perylene on a Nonporous Inorganic Silica Surface: Effects of Aqueous Chemistry on Sorption Rates. Environ. Sci. Technol. 28, 2184-2190. https://doi.org/10.1021/es00061a029.

Schoonraad, G.-L., Madito, M.J., Manyala, N., Forbes, P., 2020. Synthesis and optimisation of a novel graphene wool material by atmospheric pressure chemical vapour deposition. J. Mater. Sci. 55, 545-564. https://doi.org/10.1007/s10853-019-03948-0

Shang, H., Lu, Y., Zhao, F., Chao, C., Zhang, B., Zhang, H., 2015. Preparing high surface area porous carbon from biomass by carbonization in a molten salt medium. RSC Adv. 5, 75728-75734. . https://doi.org/10.1039/C5RA12406A.

Singh, N. B., Nagpal, G., Agrawal, S., Rachna. 2018. Water purification by using adsorbents: A review. Environ. Technol. Innov. 11, 187-240. doi:10.1016/j.eti.2018.05.006

Unuabonah, E.I., Olu-Owolabi, B.I., Böhm, L., Düring, R.A. 2016. Adsorption of polynuclear aromatic hydrocarbons from aqueous solution: Agrowaste-modified kaolinite vs surfactant modified bentonite. Bull. Chem. Soc. Ethiop. 30(3), 369-376. https://doi.org/10.4314/bcse.v30i3.5

Wang, J., Chen, Z., Chen, B., 2014. Adsorption of Polycyclic Aromatic Hydrocarbons by Graphene and Graphene Oxide Nanosheets. Environ. Sci. Technol. 48, 4817-4825. https://doi.org/10.1021/es405227u.

Wang, L., Niu, J., Yang, Z., Shen, Z., Wang, J., 2008. Effects of carbonate and organic matter on sorption and desorption behavior of polycyclic aromatic hydrocarbons in the sediments from Yangtze River. J. Hazard Mater. 154, 811-817. https://doi.org/10.1016/j.jhazmat.2007.10.096.

Wang, X., Andrews, L., 2006. Infrared spectral of $M(OH)_{1,2,3}$ (M= Mn, Fe, Co, Ni) molecules in solid argon and the character of first row transition metal hydroxide bonding. J. Phys. Chem. A 110, 10035-10045. https://doi.org/10.1021/jp0624698.

Wauchope, R.D., Savage, K.E., Koskinen, W.C., 1983. Adsorption-desorption equilibria of herbicides in soil: naphthalene as a model compound for entropy-enthalpy effects. Weed Sci. 31, 744–751. https://doi.org/10.1017/S0043174500070296

Weber, W.J., McGinley, P.M., Katz, L.E.A., 1992. Distributed reactivity model for sorption by soils and sediments. Conceptual basis and equilibrum assessments. Environ. Sci. Technol. 26, 1955–1962. https://doi.org/10.1021/es00034a012.

Xiao, B., Yu, Z., Huang, W., Song, J., Peng, P., 2004. Black carbon and kerogen in soils and sediments. Their roles in equilibrium sorption of less-polar organic pollutants. Environ. Sci. Technol. 38, 5842–5852. https://doi.org/10.1021/es049761i.

Xu, L., Wang, J., 2017. The application of graphene-based materials for the removal of heavy metals and radionuclides from water and wastewater. Critical Reviews in Environ. Sci. Technol. 47, 1042-1105. https://doi.org/10.1080/10643389.2017.1342514.

Yakout, S.M., Daifullah, A.A.M., 2013. Removal of selected polycyclic aromatic hydrocarbons from aqueous solution onto various adsorbent materials. Desalin. Water Treat. 51, 6711-6718. https://doi.org/10.1080/19443994.2013.769916.

Younis, S. A., El-Gendy, N. S., El-Azab, W. I., Moustafa, Y. M. 2015. Kinetic, isotherm, and thermodynamic studies of polycyclic aromatic hydrocarbons biosorption from petroleum refinery wastewater using spent waste biomass. Desalin. Water Treat. 56, 3013-3023. https://doi.org/10.1080/19443994.2014.964331

Yu, H., Xiao, H., Wang, D. 2014. Effects of soil properties and biosurfactant on the behavior of PAHs in soil-water systems. Environ. Syst. Res. 3, 6. https://doi.org/10.1186/2193-2697-3-6

Yu, F., Ma, J., Bi, D., 2015. Enhanced adsorptive removal of selected pharmaceutical antibiotics from aqueous solution by activated graphene. Environ. Sci. Pollut. Res. 22, 4715-4724. https://doi.org/10.1007/s11356-014-3723-9.

Yu, W., Liu, T., Crawshaw, J., Liu, T., Graham, N. 2018. Ultrafiltration and nanofiltration membrane fouling by natural organic matter: Mechanisms and mitigation by pre-ozonation and pH. Water Res. 139, 353-362. https://doi.org/10.1016/j.watres.2018.04.025

Zhao, G.X., Li, J.X., Wang, X.K., 2011. Kinetic and thermodynamic study of 1-naphthol adsorption from aqueous solution to sulfonated graphene nanosheets. Chem. Eng. J. 173, 185–190. https://doi.org/10.1016/j.cej.2011.07.072